Chinese Physics Letters

EXPRESS LETTER

Fixed Points and Crossovers for the Hysteresis Scaling of Dynamic Mean-Field Models

Cite as: Jiapeng Yang *et al*. 2026 *Chin. Phys. Lett.* **43** 070002

DOI CSTR

Recommended Articles

Interplay between the Pseudogap and Superconductivity in Doped Mott Insulators: a Cluster Dynamical Mean-Field Theory Study
Jinbin Liu, Dao-Xin Yao, and Wei Wu
Chin. Phys. Lett. **42**, 080711 (2025)

Driven Critical Dynamics in the Tricitical Point
Ting-Long Wang, Yi-Fan Jiang, and Shuai Yin
Chin. Phys. Lett. **42**, 110001 (2025)

Finite-Size Scaling Behaviors of Eigen Microstates near the Critical Point
Gaoke Hu, Jia-Qi Dong, Yongwen Zhang, Teng Liu, Wen-Long You, Maoxin Liu, and Xiaosong Chen
Chin. Phys. Lett. **43**, 020001 (2026)

Dynamical t/U Expansion of the Doped Hubbard Model
Wenxin Ding, and Rong Yu
Chin. Phys. Lett. **41**, (2024)

Localization Dynamics at the Exceptional Point of Non-Hermitian Creutz Ladder
S. M. Zhang, T. Y. He, and L. Jin
Chin. Phys. Lett. **41**, (2024)

Learning-at-Criticality in Large Language Models for Quantum Field Theory and Beyond
Xiansheng Cai, Sihan Hu, Tao Wang, Yuan Huang, Pan Zhang, Youjin Deng, and Kun Chen
Chin. Phys. Lett. **42**, 120002 (2025)

iopscience.iop.org/cpl | cpl.iphy.ac.cn

A series journal of Chinese Physical Society distributed by IOP Publishing

Chinese Physics Letters

Chin. Phys. Lett. 43 070002 (2026)

EXPRESS LETTER

DOI: 10.1088/0256-307X/43/7/070002
CSTR: 32039.14.0256-307X.43.7.070002

Fixed Points and Crossovers for the Hysteresis Scaling of Dynamic Mean-Field Models

Jiapeng Yang and Fan Zhong*

School of Physics and State Key Laboratory of Optoelectronic Materials and Technologies, Sun Yat-sen University, Guangzhou 510275, China

*Corresponding author. Email: stszf@mail.sysu.edu.cn

Phase transitions are divided into first-order and continuous ones in the current classification. While the latter shows striking phenomena of scaling and universality, the former is typically characterized by discontinuous jumps in extensive variables and pronounced hysteresis. Recent studies have demonstrated universal scaling behavior controlled by a cubic fixed point in first-order phase transitions. However, more recent investigations of hysteresis in a dynamic mean-field quartic model driven across its first-order phase transitions have revealed new scaling exponents for different driving rates. Here, we discover a new exponent for large driving rates arising surprisingly from critical phenomena and show that, depending on the magnitude of the driving rates and the absence or presence of noise, the same mean-field model remarkably exhibits several universality classes with definite universal scaling exponents governed by their corresponding fixed points, as revealed through a systematic scaling analysis based on renormalization group theory. The theories, the various crossovers between different fixed points, and the complete universal scaling of full curve collapse, are all verified by numerical results. This further confirms universal scaling in first-order phase transitions.

According to a modern classification [1], phase transitions are divided into first-order phase transitions (FOPTs) and continuous ones. While it is well known that the latter is characterized by universality and scaling near their critical points [2–5], whether FOPTs [6–9] also exhibit universal scaling behavior similar to their continuous counterparts is a long sought question [10].

A characteristic of FOPTs is hysteresis, which usually occurs when an FOPT is driven with a finite rate through its equilibrium transition point. A typical example is the magnetization of a ferromagnet in which the magnetization changes from one orientation (phase) to the other when an externally applied field is varied. Power-law scaling of FOPTs and hysteresis with respect to the field parameters has long been reported both experimentally and theoretically [10–67]. In this paper we will focus on mean-field models only. For a noiseless mean-field quartic ϕ^4 model, the dependence of the magnetic hysteresis on the field driving rate R can be exactly solved near a spinodal giving rise to coercivity scaling with an exponent, referred to as hysteresis (scaling) exponent below, of 2/3 [16], in agreement with numerical results [24,25,43,44] and that of field-like thermal transitions [51]. However, when there is noise, numerical calculations several years ago found good power-law scalings over three orders of magnitude variation of the rate but with nonuniversal exponents depending on the noise strength [57], consistent with a previous finding that no single power law exists [20]. Yet, devising a method of complete universal scaling whereby all parameters are coordinately rescaled, it has been shown that all hysteresis curves themselves can be completely collapsed onto one another using universal exponents including the aforementioned 2/3 governed by a spinodal fixed point, indicating that the nonuniversal exponents are only effective when contributions from other parameters are neglected [58,59]. Recently, it was found that apart from the 2/3 exponent, the hysteresis also exhibits 1 and 1/2 exponents for small and large driving rates, respectively [62–64]. Here, we will show that these exponents, with 1/2 replaced by a new one 3/5 found herein and arising unexpectedly from critical phenomena, are controlled by different fixed points, with crossovers between them, in the same single quartic mean-field model using a systematic scaling analysis based on renormalization-group theory. The underlying reason is that the magnitude of the driving rate and the noise strength can alter the relative dominance of different terms in the model. Specifically, at high noise levels or low driving rates, the system is dominated by the quadratic term because of sufficient fluctuations; whereas at high driving rates, the order parameter is rapidly driven to large values, making the quartic term dominant. These then result in the two new exponents. We also find that every fixed point in the mean-field theories can yield full curve collapse in all regimes controlled by different fixed points, including the crossovers between them, due to the absence of anomalous dimensions [2–5].

Consider a general model free energy

$$f_n(\phi) = \frac{1}{2}a_2\phi^2 + \frac{1}{n}a_n\phi^n - H\phi \tag{1}$$

for an order parameter ϕ and its ordering field H, where a_2 is a reduced temperature and a_n a general coupling constant. For $n = 4$, the conventional quartic ϕ^4 model exhibits a continuous transition at $a_2 = 0$ and $H = 0$ but FOPTs for all $a_2 < 0$ between two ordered phases with $\phi_{\rm eq} = \pm\sqrt{-a_2/a_4} = \pm M_{\rm eq}$ at $H = 0$. Dynamics can be studied by the usual Langevin equation [68]

$$\frac{\partial\phi}{\partial t} = -\frac{\partial f_n}{\partial\phi} + \zeta = -(a_2\phi + a_n\phi^{n-1} - H) + \zeta, \tag{2}$$

where ζ is a Gaussian white noise whose averaged moments satisfy

$$\langle\zeta\rangle = 0, \quad \langle\zeta(t)\zeta(t')\rangle = 2\sigma\delta(t-t'), \tag{3}$$

with a noise amplitude σ and we have set the conventional kinetic coefficient to unity as the time unit. Let the external field vary linearly with time as $H = H_{\rm in} + Rt$ with an initial field $H_{\rm in}$ and a constant rate R. Again for $n = 4$, the transition from $-M_{\rm eq}$ to $M_{\rm eq}$ occurs not at the equilibrium point $H = 0$, but is delayed to a larger field $H > 0$. This is hysteresis that increases with the rate R, since the system is farther out of equilibrium. Moreover, in a noiseless system, the transition can only take place beyond the so-called spinodal point ($H_{\rm s}$, $M_{\rm s}$), at which the free energy barrier between the two phases vanishes. As such, let $\phi = M_{\rm s} + \varphi$, one finds $f_4(\phi) = f_4[M_{\rm s}] + f_3(\varphi) + a_4\varphi^4/4$ [43,44] with

$$f_3(\varphi) = \frac{1}{2}\tau\varphi^2 + \frac{1}{3}a_3\varphi^3 - h\varphi, \tag{4}$$

Received 1 May 2026; accepted 22 June 2026; published 7 July 2026

© 2026 Chinese Physical Society and IOP Publishing Ltd. All rights, including for text and data mining, AI training, and similar technologies, are reserved.

Check for updates

where

$$\tau = a_2 + 3a_4M_s^2, \quad h = H - H_s, \quad a_3 = 3a_4M_s, \tag{5}$$

the first two being an effective reduced temperature and an effective field, respectively, that become zero exactly at $M_s = \pm\sqrt{-a_2/3a_4}$, and $H_s = a_2M_s + a_4M_s^3 = 2a_2M_s/3$. Therefore, $\tau = 0$ and $h = 0$ exactly at the spinodal point, similar to $a_2 = 0$ and $H = 0$ at the critical point. This gives rise to a cubic ϕ^3 theory near the spinodal where the quartic term is negligible. The dynamic equation becomes

$$\mathrm{d}\varphi/\mathrm{d}t = -(\tau\varphi + a_3\varphi^2 - h) + \zeta. \tag{6}$$

In the absence of the noise, Eq. (6) can be analytically solved by Airy's functions whose argument is proportional to $R^{-2/3}h$ for $h = Rt$. This gives rise to the exact mean-field 2/3 hysteresis exponent [16].

To see how this and other exponents emerge generally, we make a scale transformation to the dynamic equation, Eq. (2) [5,43,58]. This is to change every quantity O to O' through $O = O'b^{-[O]}$ for a scaling factor b, where we have utilized the square brackets to denote the scale dimension. To keep the transformed dynamic equation identical with the original one, one must have $[t] = -[a_2]$, $[H] = [\phi] + [a_2]$, $[\zeta] = [\phi] - [t]/2 = [\sigma]/2$, and $[a_n] = [a_2] - (n-2)[\phi]$. According to the renormalization-group theory [2–5], the Gaussian fixed point of a ϕ^n theory is reached by setting $[a_n] = 0$. This yields

$$[\phi] = \frac{1}{n-2}[a_2],\ [H] = \frac{n-1}{n-2}[a_2],\ [\sigma] = \frac{n}{n-2}[a_2] \tag{7}$$

together with $[t] = -[a_2]$. The original and transformed equations must share the same solution since they are identical. Accordingly,

$$\phi = b^{-[\phi]}\phi\left(a_2b^{[a_2]}, a_nb^{[a_n]}, Hb^{[H]}, tb^{[t]}, \sigma b^{[\sigma]}\right). \tag{8}$$

We then choose $H_{\mathrm{in}} = -Rt_0$ and shift t by t_0, i.e., $t - t_0 \to t$ so that $H = Rt$. Next, we change the variable from t to R, and set $b = R^{-1/r}$, where $r \equiv [R]$ satisfies [69]

$$r = [H] - [t] = (2n-3)[a_2]/(n-2). \tag{9}$$

These lead to the finite-time scaling (FTS) forms [69–71],

$$H = R^{\frac{n-1}{2n-3}}g_n\left(a_2R^{-\frac{n-2}{2n-3}}, a_n, MR^{-\frac{1}{2n-3}}, \sigma R^{-\frac{n}{2n-3}}\right), \tag{10}$$

where g_n (applicable to both a general n and each specific value in the equations below) is a universal scaling function and $M = \langle\phi\rangle$ the order parameter averaged over the noise. Note that we have expressed H as a function of M. The reason why Eq. (10) is referred to as an FTS form is that $R^{[t]/r} = R^{-z/r}$ [derived from $tR^{-[t]/[r]}$ by substituting $b = R^{-1/r}$ into Eq. (8)] is an externally imposed finite driving timescale, in direct analogy with the finite system size in finite-size scaling. This controllable finite timescale allows one to circumvent critical slowing down, just as the finite size allows one to overcome divergent correlation lengths [69–73].

Equation (10) describes the general, systematic dependence of H on R and other parameters. This is the advantage of the renormalization-group analysis over direct approximations to the dynamic equation that usually just produce approximate relations to one specific parameter rather than the whole scaled variables. From Eq. (10), we obtain the leading hysteresis exponent as $(n-1)/(2n-3)$, taking on values 1, 2/3, 3/5, and 1/2 for $n = 2$, 3, 4, and ∞. It decreases from 1 to 1/2 as n increases from 2 to infinity. Moreover, the corresponding FTS forms are

$$H = Rg_2(a_2, a_4R^2, MR^{-1}, \sigma R^{-2}), \tag{11}$$

$$H = R^{2/3}g_3(a_2R^{-1/3}, a_4R^{1/3}, MR^{-1/3}, \sigma R^{-1}, a_3), \tag{12}$$

$$H = R^{3/5}g_4(a_2R^{-2/5}, a_4, MR^{-2/5}, \sigma R^{-4/5}), \tag{13}$$

$$H = R^{1/2}g_\infty(a_2R^{-1/2}, a_4R^{-1/2}, M, \sigma R^{-1/2}, a_\infty) \tag{14}$$

by substituting the specific n values. In Eqs. (11)–(14), besides Eq. (13), we also keep the scaled variable associated with a_4 in all other equations since we will numerically solve Eq. (2) for $n = 4$. The corresponding exponent can be derived from $[a_4] = [a_3] - [\phi]$ for $n = 3$ using Eq. (5) and $[a_4] = [a_2] - 2[\phi]$ from the expression for general n. Indeed, for $n = 2$, $[a_2] = 0$ and so $[a_4] = -2[\phi]$, dictating the exponent relation between a_4 and M, while for $n = \infty$, $[\phi] = 0$ and thus $[a_4] = [a_2]$, indicating that a_4 and a_2 share the same exponent. We have used H and M to express the scaling form for $n = 3$ in Eq. (12). However, to observe the real cubic behavior, one must employ Eqs. (4) and (5), resulting in

$$h = R^{2/3}g_3'(a_2R^{-1/3}, a_4R^{1/3}, mR^{-1/3}, \sigma R^{-1}, a_3), \tag{15}$$

where g_3' is a scaling function different from g_3 and we have used directly a_2 instead of τ since they differ only by a constant of identical dimension [58]. From Eqs. (11)–(15), it is important to note that the exact hysteresis exponents can only be obtained if all the arguments in the scaling functions are kept constant; otherwise, effective exponents that depend on the parameters and R result. In the following, we describe the mean-field behavior represented by each FTS form in Eqs. (11)–(15), characterized by the marginal (dimensionless) a_n and its corresponding Gaussian fixed point. This might suggest requiring a series of distinct models, each with its own highest order term a_n. Remarkably, however, we find that these FTS forms, except for the infinite-order case, collectively capture the distinct behaviors of the single quartic ϕ^4 model itself across different R and under both noisy and noiseless conditions. Moreover, they are all shown below to be complete scaling forms in the sense that no parameter in the forms can be dropped and no additional parameter is needed in order to produce full curve collapse, or complete universal scaling.

We now examine the FTS forms, Eqs. (11)–(14), which will be referred to as the quadratic, cubic, quartic, and infinite-order behavior, respectively, for definite. First comes the quadratic behavior Eq. (11) in which the highest order term needed is a_2 corresponding to a quadratic ϕ^2 model. The dynamic equation reduces to

$$\mathrm{d}\phi/\mathrm{d}t = -a_2\phi + H + \zeta. \tag{16}$$

Indeed, one sees from Eq. (11) that a_4 is irrelevant and becomes negligible for $R \to 0$. A normal situation this model describes is a paramagnet (the disordered phase) for $a_2 > 0$ or $T > T_c$, the Curie temperature. From Eq. (16), the equation of state is then simply $H = a_2M$ and the susceptibility is proportional to $1/a_2$, which is just Curie-Weiss' law. The hysteresis depends linearly on R, giving rise to an exact hysteresis exponent 1, which can also be derived from the analytical solution of Eq. (16) for $H = Rt$. Another situation in which this model is applicable occurs when the noise amplitude σ is large enough so that the system makes a transition to a regime in which it can freely jump from one potential well to the other for $a_2 < 0$ [28]. As a result, the averaged magnetization is so small that the quadratic ϕ^2 term is sufficient in this high-noise regime, leading again to the linear scaling observed recently [62–64].

One might imagine yet another situation for such small driving rates that the transition is close to the equilibrium transition point at $H = 0$ and $a_2 < 0$. If, in contrast to the above situation, the averaged magnetization could keep its mean-field value and so would not be small. We could then expand M around M_{eq} at $H = 0$, arriving at

$$\frac{\mathrm{d}m}{\mathrm{d}t} = -(a_2 + 3a_4M_{\mathrm{eq}}^2)m - H + \zeta = 2a_2m - H \tag{17}$$

to the leading order. Note that the coefficient of the linear term in Eq. (17) is finite, different from the cubic ϕ^3 model at the spinodal point Eq. (4), and twice as large as the coefficient of the original quadratic ϕ^2 model, Eq. (16). In fact, these two quadratic models represent the lowest order behaviors of the ordered phase and the disordered phase, whose susceptibilities have a universal amplitude ratio of 2 at the mean-field level [2–5]. The FTS scaling of this low-rate regime would change to

$$H = Rg_2(a_2, a_4R^2, (M - M_{\mathrm{eq}})R^{-1}, \sigma R^{-2}). \tag{18}$$

Therefore, one could again have a ϕ^2 theory with a linear scaling. However, at least for the present mean-field model which lacks nucleation,

Table 1. Fixed points, asymptotic behaviors, and their crossover exponents ρ for various representations using Eqs. (11)–(15) in the absence of noise.

#	Representations	$R \to 0$, $H \to H_s$, cubic fixed point		$R \to \infty$, $H \to R^{3/5}$, quartic fixed point	
		Behavior	ρ	Behavior	ρ
1	HR^{-1} versus a_4R^2	$(a_4R^2)^{-1/2}$	$-1/2$	$(a_4R^2)^{-1/5}$	$-1/5$
2	$HR^{-2/3}$ versus $a_2R^{-1/3}$	$(a_2R^{-1/3})^2$	2	$(a_2R^{-1/3})^{1/5}$	$1/5$
3	$HR^{-2/3}$ versus $a_4R^{1/3}$	$(a_4R^{1/3})^{-2}$	-2	$(a_4R^{1/3})^{-1/5}$	$-1/5$
4	$HR^{-2/3}$ versus $(a_2/a_4)R^{-2/3}$	$[(a_2/a_4)R^{-2/3}]^1$	1	$[(a_2/a_4)R^{-2/3}]^{1/10}$	$1/10$
5	$HR^{-3/5}$ versus $a_2R^{-2/5}$	$(a_2R^{-2/5})^{3/2}$	$3/2$	$(a_2R^{-2/5})^0$	0
6	$HR^{-1/2}$ versus $a_4R^{-1/2}$	$(a_4R^{-1/2})^1$	1	$(a_4R^{-1/2})^{-1/5}$	$-1/5$

M does not retain its mean-field value but becomes smaller for sufficiently small rates. Accordingly, Eq. (18) does not apply to the model itself, but may be applicable to scenarios requiring nucleation.

Next we study the cubic behavior Eq. (12) for the cubic ϕ^3 theory where a_3 is marginal. As constructed in Eq. (4), this theory characterizes the behavior of the transition in the vicinity of the spinodal point (H_s, M_s) within the noiseless quartic ϕ^4 model. For the corresponding noisy model, the transition can occur prior to reaching H_s due to noise activation. Crucially, any finite noise can trigger the transition because the mean-field nature of the model requires no nucleation. One can still estimate a noise-shifted spinodal near which the cubic theory ought to be valid again. On the basis of this idea, it has been shown that all curves of different R values can indeed collapse onto each other if all parameters of the original quartic model are consistently rescaled according to the FTS form, Eq. (12) [58]. This indicates that the observed noise-strength dependent hysteresis exponents [57] are effective, because contributions from scaled variables other than $hR^{-2/3}$ in Eq. (12) or (15) were not considered. Additionally, the 2/3 hysteresis exponent has also been observed in the intermediate R range by expanding the dynamic equation, Eq. (2), around a reference point (H_p, R_p) [63,64].

Now we consider the quartic behavior Eq. (13) for the quartic model. This is the standard mean-field model for critical phenomena near the critical point $a_2 = 0$ and $H = 0$ [43,58]. However, at sufficiently large R values, M is large enough that the quadratic a_2 term can be neglected compared to the a_4 term, leading to effective criticality. The hysteresis of the FOPTs is therefore unexpectedly captured by the critical ϕ^4 theory for continuous phase transitions, yielding the leading hysteresis exponent of 3/5.

Finally comes the infinite-order behavior Eq. (14) in which a_∞ is marginal. For very large R, M is rapidly driven to large values and hence the highest order term a_∞ is dominant, which in practice may be approximated by using a very large n. The leading hysteresis exponent ought to be 1/2. However, for the ϕ^4 theory, the highest-order term is only a_4. As a result, the FTS of the hysteresis must be described by Eq. (13) and the leading hysteresis exponent must be 3/5 instead.

We have seen that different R ranges can be controlled by different fixed points. This indicates that crossovers between different regimes—controlled by their respective fixed points—are inevitable over a wide range of R values. For a noiseless quartic ϕ^4 model, two distinct regimes exist: one as $R \to 0$, controlled by the cubic fixed point, and the other as $R \to \infty$, governed by the quartic fixed point, corresponding to small and large R values, respectively. This means that if one plots some characteristic loci of the magnetization curves over a wide range of R values using any scaling form from Eqs. (11)–(15), the resultant curves must exhibit the two distinct regimes and a crossover between them. For example, if one plots HR^{-1} versus a_4R^2 at $M = 0$ according to Eq. (11), the resulting curves are expected to scale as $(a_4R^2)^{-1/2}$ and $(a_4R^2)^{-1/5}$ so that $H \to H_s$ and $H \to R^{3/5}$ in the limits $R \to 0$ and $R \to \infty$, respectively. The exponents $-1/2$ and $-1/5$ are termed crossover (or more precisely, trans-regional) exponents that are determined to yield the correct asymptotic behaviors. We summarize the results for various representations using Eqs. (11)–(15) in entries labeled #1–#6 in Table 1. We have presented in entries #2 and #3 of Table 1 two different representations for $n = 3$. In fact, they can be consolidated into a single form, shown in entry #4. For completeness, entry #6 gives the representation for $n = \infty$, Eq. (14). Note that all but the last entry #6 refer to the quartic model, and the 0 crossover exponent in #5 of Table 1 indicates that the regime is described by the quartic fixed point itself. Note also that for $R \to 0$, $H \to H_s$, the spinodal field.

To explicitly observe the cubic behavior, we have to work at the spinodal point (H_s, M_s) according to Eq. (15). Therefore, one can find by interpolation, instead of the coercivity H_c at $M = 0$, the field H_0 at $M = M_s$, which approaches H_s as $R \to 0$. Plateaux ought to emerge for small R following Eq. (15), representing the cubic behavior. It then crossovers to the large-R 3/5 behavior governed by the quartic fixed point similar to entries #2 and #3 in Table 1. However, as the scaled arguments are now associated with h and m instead of H and M, the crossover to the quartic behavior described by Eq. (15) is less neat compared to Eq. (12). Nevertheless, sufficiently far away from the crossover region, the behaviors in different regimes are expected to follow those of H listed in Table 1 for $H_0 - H_s$ as well.

For a noisy ϕ^4 model, in addition to the two regimes for the noiseless model, emerges a third regime—the high-noise regime—described by Eq. (11) governed by the quadratic fixed point for $R \to 0$. There are then new crossovers between this regime and the cubic or quartic regimes, which may emerge for small, intermediate, and large R, respectively, depending on the model parameters. These crossovers are collected in Table 2, where we have used the consolidated form for the cubic behavior (the individual form doubles the crossover exponents). Note that in the intermediate cubic regime H approaches a noisy H_s.

Two remarks are in order. First, when the barrier between the considered two phases is large compared to the noise strength, the high-noise regime may require too small rates to be practically executable within reasonable computation time for solving Eq. (2). In this case, the quadratic behavior is absent and hysteresis plateaux are observed [63,64]. The hysteresis behavior is then similar to the noiseless case, including the corresponding crossovers given by in Table 1.

Second, as mentioned above, the real cubic behavior can only be probed at the spinodal point, which, however, is not exactly solvable for a noisy system. As an estimation, we employ the Kramer rate formula [74,75]

$$\mathcal{K} = \frac{\omega_0 \omega_b}{2\pi} \exp\{-\Delta E_b/\sigma\}, \tag{19}$$

for an overdamped particle attempting to escape from a metastable potential well over a barrier ΔE_b with angular frequencies ω_0 and ω_b, respectively, given by the square root of the absolute value at the corresponding second derivative of the potential. The scale-dependent spinodal H_s (we use the same symbol for both noiseless and noisy systems) is then estimated with the criterion [10]

$$1/\mathcal{K} = cR^{-z/r}, \tag{20}$$

namely, the escaping time $1/\mathcal{K}$ is proportional to the driving time $R^{-z/r}$ with a ratio c. One may compute the magnetization at this estimated spinodal, fit its R-dependence, and thereby determine the corresponding M_s following Eq. (15). However, since Eq. (15) involves

Table 2. Fixed points, asymptotic behaviors and their crossover exponents ρ for three representations corresponding to the quadratic, cubic, and quartic behaviors in the presence of noise.

#	Representations	$R \to 0$, $H \to R$ quadratic fixed point		Intermediate R, $H \to H_s$ cubic fixed point		$R \to \infty$, $H \to R^{3/5}$ quartic fixed point	
		Behavior	ρ	Behavior	ρ	Behavior	ρ
1	HR^{-1} versus a_4R^2	$(a_4R^2)^0$	0	$(a_4R^2)^{-1/2}$	$-1/2$	$(a_4R^2)^{-1/5}$	$-1/5$
2	$HR^{-2/3}$ versus $(a_2/a_4)R^{-2/3}$	$[(a_2/a_4)R^{-2/3}]^{-1/2}$	$-1/2$	$[(a_2/a_4)R^{-2/3}]^1$	1	$[(a_2/a_4)R^{-2/3}]^{1/10}$	1/10
3	$HR^{-3/5}$ versus $a_2R^{-2/5}$	$(a_2R^{-2/5})^{-1}$	-1	$(a_2R^{-2/5})^{3/2}$	3/2	$(a_2R^{-2/5})^0$	0

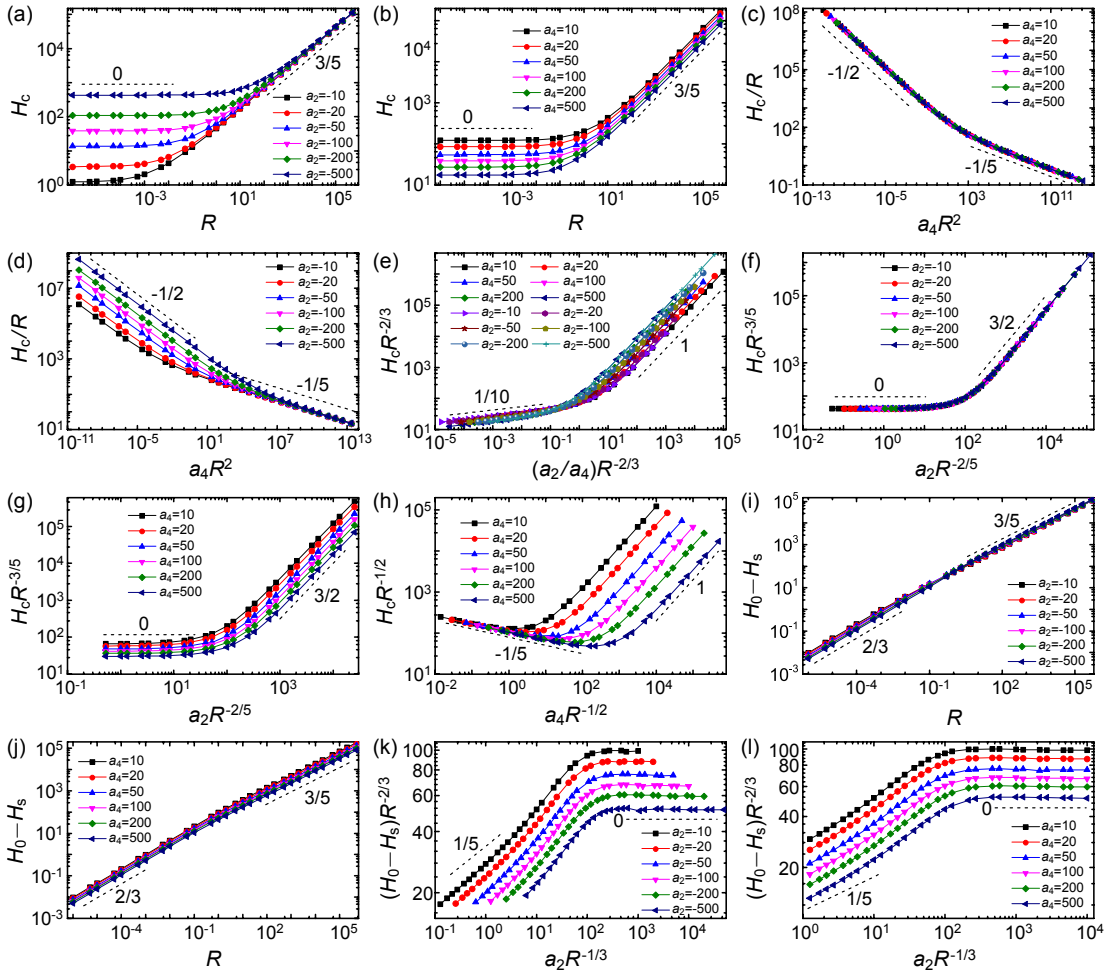

Fig. 1. (a) Coercivity H_c versus R at fixed $a_4 = 100$ with varying a_2. (b) H_c versus R at fixed $a_2 = -100$ with varying a_4. Both (a) and (b) correspond to $\sigma = 0$. Dashed lines with numerical labels in all panels indicate the theoretical (crossover) slopes from Table 1. (c) and (d) Quadratic rescaling of (a) and (b) by Eq. (11). (e) Cubic rescaling of (a) and (b) using the consolidated form of Eq. (12). (f) and (g) Quartic rescaling of (a) and (b) by Eq. (13). (h) Infinite-order rescaling of (b) by Eq. (14). (i) and (j) $H_0 - H_s$ at M_s versus R for the same parameter sets as in (a) and (b). (k) and (l) Cubic scaling of (j) and (k) by Eq. (15). Lines connecting symbols are only a guide to the eye.

other rate-dependent scaled variables that remain unfixed, such direct fits are inevitably inaccurate, similar to usual procedures for determining hysteresis exponents. As a compromise, for a given c and its derived H_s, we plot the cubic rescaling of $(H - H_s)R^{-2/3}$ as a function of $a_2R^{-1/3}$ for all $H > H_s$ on a magnetization curve and directly search for a point where the slope matches the theoretical slope expected for a regime (given in Table 2) according to whether it is cubic, quadratic, or quartic. The M value at this point is identified as M_s, and the corresponding H value is H_0 [76]. Although this seems *ad hoc* and the estimated spinodal may not be unique, its existence is consistent with the theory and thus confirming it.

The noiseless dynamic equation, Eq. (2), can be quite accurately solved using existing numerical schemes such as Runge–Kutta methods. For the noisy equation, we use explicit Euler discretization with a time step as small as 2.5×10^{-7} for the largest $R = 500000$, and up to 0.01 for smaller R to ensure stability of the solution. It is important to choose an initial field H_{in} sufficiently far away from the real transition point (e.g., the coercivity) to ensure independence from the initial conditions. 25000 samples were used for averaging.

We show the dependence of H_c on R for the noiseless quartic model in Figs. 1(a) and 1(b) for fixed a_4 and a_2 but various a_2 and a_4, respectively. It is apparent that the slopes approach 0 and 3/5 for small R and large R, respectively. This indicates that the system tends to constants for small R and the behavior controlled by the quartic fixed point at large R. To confirm this, in Figs. 1(c) and 1(d) we depict the scaling plots following the quadratic behavior Eq. (11). One observes that H_c for all R and all a_4 collapses remarkably onto a single curve at fixed a_2, confirming that the quadratic behavior originates from fixed a_2. Meanwhile, the curves for different a_2 tend to distinct parallel lines at small R but converge at large R—consistent

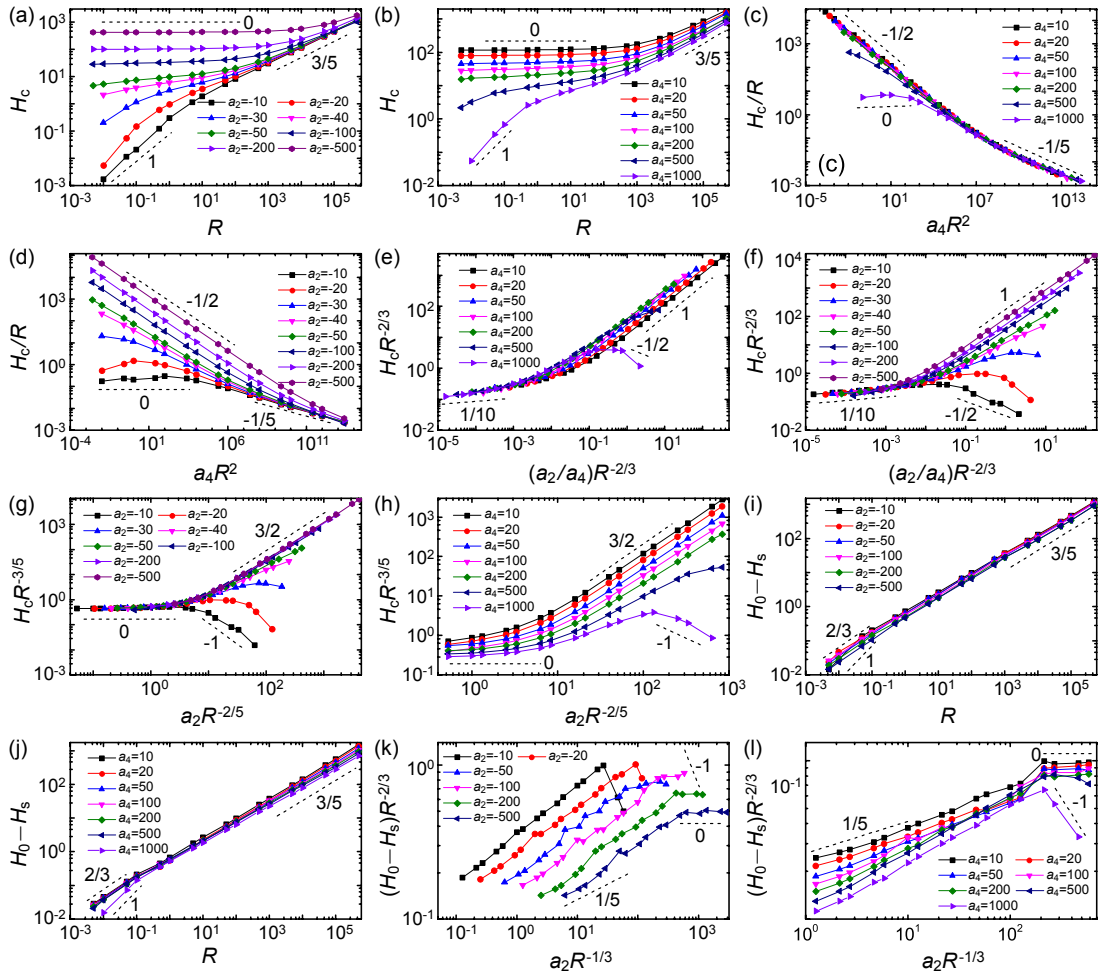

Fig. 2. (a) and (b) H_c versus R for the same parameters as (a) and (b) in Fig. 1 but with $\sigma = 0.4$. Lines and symbols are as in Fig. 1. (c)–(h) Rescaling of (a) and (b) following Eqs. (11)–(13). (i) and (j) $H_0 - H_s$ at the noisy M_s for identical parameter sets to (a) and (b) using $c = 50\pi$. (k) and (l) Cubic rescaling of (i) and (j) by Eq. (15).

with Eq. (11) since g_2 depends on a_2. Moreover, both small-R and large-R regimes are sloped lines (not horizontal), with corresponding slopes of $-1/2$ and $-1/5$. These values match the crossover exponents in #1 of Table 1, which governs crossovers to the constant H_s at small R and the 3/5 scaling at large R. Similarly, scaling plots are shown for the cubic behavior in Fig. 1(e), the quartic behavior in Figs. 1(e) and 1(f), and the infinite-order behavior in Fig. 1(g). Again, H_c for all R and all a_2 falls onto a single curve at fixed a_4, while curves of different a_4 remain parallel, as shown in Figs. 1(f) and 1(g). All curves exhibit two linear segments, whose slopes agree with the crossover exponents in Table 1. Horizontal lines appear only in Figs. 1(f) and 1(g), correctly reflecting the quartic behavior at large R. All other linear segments are oblique, representing crossovers to either the large-R 3/5 scaling or the small-R constant H_s.

To explicitly reveal the leading R-dependence of the approach to H_s, we first find the field H_0 at M_s instead of H_c at $M = 0$ and show its dependence on R in Figs. 1(i) and 1(j). One sees two linear segments with slopes of 2/3 and 3/5 for small and large rates, respectively. Indeed, through the cubic rescaling of H_0 by Eq. (15) in Figs. 1(k) and 1(l), the plateaux at small R, as expected, emerges consistent with the cubic behavior with the 2/3 hysteresis exponent. The large R portion exhibits a slope of about 1/5 in agreement with the crossover to the quartic behavior, entry #2 in Table 1. However, the agreement and linearity for large R are not as good as those in Fig. 1(e) (note the half slope due to the consolidated form) owing to the two terms $H_sR^{-2/3}$ and $M_sR^{-1/3}$ implied in Eq. (15). Only when R is so large that these two terms become negligible does the quartic behavior emerge.

We have shown both from the theory and from the numerical results that the large R behavior is the quartic 3/5 critical scaling, different from the 1/2 behavior found in Refs. [63,64]. The infinite-order rescaling in Fig. 1(h) confirms the absence of such a behavior through the absence of a plateau. It is probably an effective exponent arising from the initial conditions, which lead to additional scaled variables in the scaling functions if the system is not in quasi-equilibrium, as analyzed in Ref. [72]. The H_{in} was chosen to be near the symmetrically opposite point of H_s; this choice is not sufficient for large rates, because M will increase directly instead of stabilizing for some time in the metastable state following a short transient. Further evidence for the effectiveness of 1/2 is that it lies between 0 and 3/5, the range of exponent values in Figs. 1(a) and 1(b).

When the noise strength is finite, the dependence of H_c on R is distinct, as shown in Figs. 2(a) and 2(b) for a series of a_2 and a_4, respectively, with fixed σ. One sees that, besides the large-R 3/5 scaling and the small-R plateaux, for a_2 so large or a_4 so small that the equilibrium barriers between the two phases $a_2^2/2a_4$ are small, the small R portions exhibit linear decreases. This linearity at $M = 0$ rather than M_{eq} rules out Eq. (18) as its origin. In addition, small rather than equilibrium M is evident in Ref. [64]. We present H_c in terms of the quadratic behavior in Figs. 2(c) and 2(d), cubic behavior in Figs. 1(e) and 2(f), and quartic behavior in Figs. 2(g) and 2(h). The main curves in all these figures are similar to the corresponding noiseless behaviors in Figs. 1(c)–1(g) [Fig. 1(e) is separated into Figs. 2(e) and 2(f) for clarity], except that some curves in these figures gradually deviate from the main curves as the barriers between the two phases are lowered. The curves exhibiting large deviations show plateaux at small R under the quadratic rescaling, thus confirming the linear

scaling. At large R, they converge to the main curves, which exhibit lines with slopes of $-1/5$, $1/10$, and 0 under the quadratic, cubic, and quartic rescaling, respectively. This is in accordance with the 3/5 scaling behavior listed in the last column of Table 2, similar to the noiseless case. At small R, the main curves show lines with slopes of $-1/2$, 1, and $3/2$ for the quadratic, cubic, and quartic rescaling, respectively, which are consistent with the crossover exponents in the middle column in Table 2, and are again identical to those of the noiseless cases. This agrees with the plateaux of the main curves at small R in the original Figs. 2(a) and 2(b).

The identical features exhibited by the main curves in Figs. 2(c) and 2(d) (excluding curves showing the additional quadratic behavior) as compared to Figs. 1(c)–1(g) for the noisy and noiseless behaviors unequivocally demonstrate that the plateaux in Figs. 2(a) and 2(b) must originate from the cubic fixed point for the spinodal. We therefore employ Eqs. (19) and (20) to estimate the noisy H_s and M_s [76]. The resultant $H_0 - H_s$ vs R is depicted in Figs. 2(i) and 2(j). Two distinct slopes of 3/5 and 2/3 at the large and small R regimes are evident. Even the linear 1 slope is discernible at small R for the quadratic behavior of large a_2 and a_4. Cubic rescaling of $H_0 - H_s$ is displayed in Figs. 2(k) and 2(l). Plateaux for small R emerge and transition to the quartic 3/5 regime with a slope of $1/5$ given by entry #2 in Tables 1 and 2 (note the half slope due to the consolidated form). Crossing over from the cubic to quadratic behavior of the slope -1, entry #2 in Table 2, is visible for $a_4 = 500$ in Fig. 2(l) and ought to be evident from the gradual deviation from the main curves in Figs. 2(a) and 2(b). Direct crossovers from the quartic to quadratic behavior, with respective slopes of $1/5$ and -1 as per entry #2 in Table 2, and hence the absence of the cubic behavior, are also manifest in Figs. 1(k) and 1(l). However, this crossover appears abrupt since the data points can be selected with some degree of freedom. We simply display several representative data points as an illustration of the capacity of the current method to detect even the presence of the quadratic regime. We emphasize, nevertheless, that the crossover is unequivocal as shown in Figs. 2(a)–2(h). Moreover, the range of c values that can lead to reasonable M_s for all parameters considered is not arbitrary but is restricted to $20\pi \lesssim c < 200\pi$, even though H_s depends on c.

We have seen that all the scaling forms, Eqs. (11)–(15), describe well all their respective regimes and the crossovers. One can then fix all scaled arguments in the scaling functions except for one and collapse all curves of different R values. This has been performed in Ref. [58] and confirmed in Ref. [64]. All the whole magnetization curves of all R values—both large and small—collapse onto one another using Eq. (12) for both the noiseless and noisy quartic model and thus was termed complete universal scaling [58]. However, as we have shown that the large and small R regimes across an extended R range may also obey distinct scaling behaviors, we therefore further investigate this complete universal scaling here.

As an example, we show in Fig. 3(a) the magnetization curves for a series of R values spanning over more than 11 orders of magnitude, with $a_2 R^{-1/2}$, $a_4 R^{-1/2}$, and σ fixed to those of a reference curve. The range is so large that the curves at small rates appear crowded together. After being rescaled according to the infinite-order scaling Eq. (14), all curves in Fig. 3(a) completely collapse onto one another as illustrated in Fig. 3(b). This is because $HR^{-1/2} = g_\infty(a_{20}R_0^{-1/2}, a_{40}R_0^{-1/2}, M, \sigma_0 R_0^{-1/2}, a_\infty)$, i.e., $HR^{-1/2}$ is only a function of M and does not depend on R, since all other variables are constant. Note that the curves are solutions of the quartic model, Eq. (2), rather than of an infinite-order model. However, once the curves are rescaled with the scaled variables fixed according to the infinite-order scaling, Eq. (14), they coincide completely, regardless of the regimes, the crossovers between them, as well as of whether the regimes are dominated by the quadratic, cubic, or quartic fixed point. We have checked that similar result applies to all other scaling forms for both noiseless or noisy systems. Therefore, any scaling form in Eqs. (11)–(14) can completely collapse all curves in all regimes and their crossovers. This is reasonable as all the scaling forms keep the dynamic equation unchanged. It

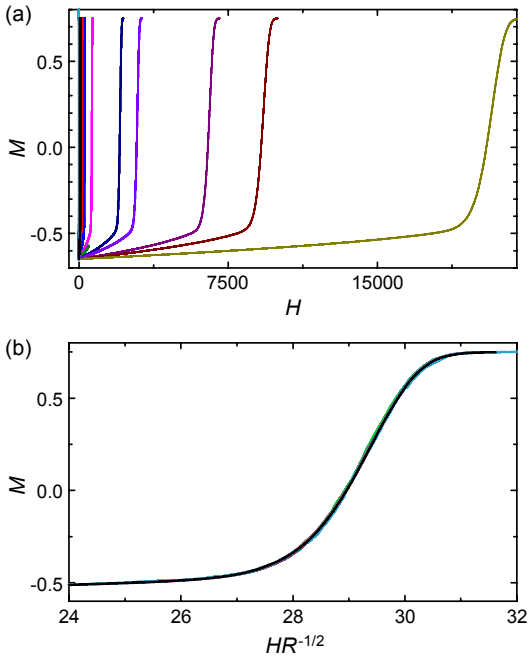

Fig. 3. (a) Magnetization curves for $R = 10^{-6}$, 5×10^{-6}, 10^{-5}, 5×10^{-5}, …, 10^5, 5×10^5 (24 curves in total). They systematically shift to the right with increasing R. $a_2 = a_{20}(R/R_0)^{-1/2}$, $a_4 = a_{40}(R/R_0)^{-1/2}$, and $\sigma = \sigma_0(R/R_0)^{-1/2}$, where $a_{20} = -400$, $a_{40} = 948$, $\sigma_0 = 0.4$, and $R_0 = 10$ are the reference curve parameters. (b) Rescaled curves from (a) based on the infinite-order scaling, Eq. (14).

is thus not possible to distinguish different regimes by complete universal scaling. However, this does not mean that the method is useless. It is a full use of the scaling forms and thus completely verifies them. Moreover, we have checked that once spatial extensions are taken into account, the anomalous dimensions lift this over-universal behavior of the mean-field theory. It can then effectively avoid approximate estimation of the noisy H_s and M_s, as demonstrated in Refs. [58–60].

We have systematically studied the dynamic quartic (ϕ^4) mean-field model driven by a linearly varying external field across its first-order phase transitions and shown that the large rate scaling exponent is 3/5, strikingly governed by the quartic fixed point in critical phenomena, contrary to the recently reported 1/2. Employing the scaling analysis based on the renormalization-group theory, we have developed systematic scaling theories for the diverse universal scaling behaviors that are remarkably exhibited by the mean-field model and controlled by distinct fixed points for various driving rates and noise conditions (absent or present). In the absence of noise, the cubic and the quartic fixed points control the small- and large-rate scaling behaviors with the leading hysteresis exponents of 2/3 and 3/5, respectively. On the other hand, in the presence of noise, the additional quadratic fixed point with the leading exponent of 1 may emerge if the driving rate is sufficiently low, while the cubic fixed point may be absent for sufficiently strong noise. Crossover features between various regimes governed by the fixed points have also been analytically described and numerically validated, thereby unequivocally confirming the theories. The spinodal points are important for the emergence of the cubic behavior and have been estimated in the noisy model. We have also demonstrated that every fixed-point scaling form can yield the complete universal scaling of full curve collapse in all different regimes and their crossovers, due to the absence of anomalous dimensions in mean-field theory. This further corroborates the scaling theories and hence universal scaling behavior in first-order phase transitions.

We have shown that even at the mean-field level, first-order phase transitions exhibit richer phenomena than continuous ones: A single mean-field model can possess distinct fixed points that lead to various

scaling behaviors. A mean-field theory is valid both for a system with long-range interactions and for a system above an upper critical dimension, which, for first-order phase transitions, is 6 [43]. Therefore, a generic mean-field type microscopic model, such as the Curie–Weiss model [63,64], and Ising-like models with short-range interactions above the upper critical dimension of 6 can both exhibit the quadratic and cubic behaviors. Regarding the large-rate scaling behavior, we have shown that it can be distinct for different values of n in ϕ^n. This explains the different large-rate scaling behaviors observed in the Curie–Weiss model [63,64] and implies that such behavior may only be analyzed case by case. However, for a model with a fixed spin size, M cannot increase indefinitely, and thus its large-rate scaling behavior is not necessarily determined by the largest order. Below the upper critical dimension, spatial fluctuations become essential. The first consequence is that nucleation is expected to change the quadratic behavior from Eq. (11) to (18) as mentioned above. However, this behavior is predicted to occur for unrealistically low rates [10]. Another consequence is that the anomalous dimensions are finite and non-mean-field exponents emerge as in the cubic [43,44] and quartic theories [2−5]. For large external fields at large driving rates, non-mean-field exponents for the quartic theory may not be needed. It is then crucial to study universal scaling of the first-order phase transitions at low and intermediate rates where the cubic fixed point dominates [10,58−61]. Detailed behavior and crossovers merit further study.

Acknowledgements

We thanked Dr. Y.-H. Ma for informing us of their initial conditions in their solutions. This work was supported by the National Natural Science Foundation of China (Grant No. 12175316).

References

[1] Fisher M E 1967 *Physics* **3** 255
[2] Ma S K 1976 *Modern Theory of Critical Phenomena* (Benjamin Canada)
[3] Cardy J 1996 *Scaling and Renormalization in Statistical Physics* (Cambridge University Press)
[4] Zinn-Justin J 2021 *Quantum Field Theory and Critical Phenomena* 5th edn (Oxford University Press)
[5] Amit D J and Martin-Mayer V 2005 *Field Theory, the Renormalization Group, and Critical Phenomena* 3rd edn (World Scientific)
[6] Gunton J D, San Miguel M, and Sahni P S 1983 *Phase Transitions and Critical Phenomena* eds. Domb C and Lebowitz J L (Academic London) **8** 267
[7] Binder K 1987 *Rep. Prog. Phys.* **50** 783
[8] Binder K and Fratzl P 2001 *Phase Transformations in Materials* ed. Kostorz G (Wiley Weinheim) p. 409
[9] Binder K and Virnau P 2016 *J. Chem. Phys.* **145** 211701
[10] Zhong F 2018 *J. Phys. Condens. Matter* **30** 445401
[11] Rayleigh J S W 1887 *Philos. Mag.* **23** 225
[12] Steinmetz C P 1892 *Trans. Am. Int. Electr. Eng.* **9** 3
[13] Rao M, Krishnamurthy H R, and Pandit R 1990 *Phys. Rev. B* **42** 856
[14] Lo W S and Pelcovits R A 1990 *Phys. Rev. A* **42** 7471
[15] Dhar D and Thomas P B 1990 *J. Phys. A* **25** 4967
[16] Jung P, Gray G, Roy R, and Mandel P 1990 *Phys. Rev. Lett.* **65** 1873
[17] Rao M and Pandit R 1991 *Phys. Rev. B* **43** 3373
[18] Sengupta S, Marathe Y, and Puri S 1992 *Phys. Rev. B* **45** 7828
[19] Somoza A M and Desai R C 1993 *Phys. Rev. Lett.* **70** 3279
[20] Mahato M C and Shenoy S R 1993 *J. Stat. Phys.* **73** 123
[21] Thomas P B and Dhar D 1993 *J. Phys. A* **26** 3973
[22] He Y L and Wang G C 1993 *Phys. Rev. Lett.* **70** 2336
[23] Acharyya M and Chakrabarti B K 1993 *Physica A* **192** 471
[24] Luse C N and Zangwill A E 1994 *Phys. Rev. E* **50** 224
[25] Zhong F, Zhang J X, and Siu G G 1994 *J. Phys. Condens. Matter* **6** 7785
[26] Jiang Q, Yang H N, and Wang G C 1995 *Phys. Rev. B* **52** 14911
[27] Zhong F and Zhang J X 1995 *Phys. Rev. E* **51** 2898
[28] Zhong F, Zhang J X, and Liu X 1995 *Phys. Rev. E* **52** 1399
[29] Hohl A, van der Linden H J C, Roy R, Goldsztein G, Broner F, and Strogatz S H 1995 *Phys. Rev. Lett.* **74** 2220
[30] Zhong F and Zhang J X 1995 *Phys. Rev. Lett.* **75** 2027
[31] Zhang J X, Zhong F, and Siu G G 1996 *Solid State Commun.* **97** 847
[32] Kim Y H and Kim J J 1997 *Phys. Rev. B* **55** R11933
[33] Suen J S and Erskine J L 1997 *Phys. Rev. Lett.* **78** 3567
[34] Chakrabarti K and Acharyya M 1998 *Rev. Mod. Phys.* **71** 847
[35] Lee W Y, Choi B C, Lee J, Yao C C, Xu Y B, Hasko D G, and Bland J A C 1999 *Appl. Phys. Lett.* **74** 1609
[36] Kuang Z Q, Zhang J X, Zhang X H, Liang K F, and Fung P C W 2000 *Solid State Commun.* **114** 231
[37] Schulke L and Zheng B 2000 *Phys. Rev. E* **62** 7482
[38] Zhong F 2002 *Phys. Rev. B* **66** 060401
[39] Park J H, Kim C S, Choi B C, Moon B K, Jeong J H, and Kim I W 2003 *Appl. Phys. Lett.* **83** 536
[40] Pan B, Yu H, Wu D, Zhou X H, and Liu J M 2003 *Appl. Phys. Lett.* **83** 1406
[41] Yıldız S, Pekcan O, Berker A N, and Özbek H 2004 *Phys. Rev. E* **69** 031705
[42] Zhu H, Dong S, and Liu J M 2004 *Phys. Rev. B* **70** 132403
[43] Zhong F and Chen Q Z 2005 *Phys. Rev. Lett.* **95** 175701
[44] Zhong F 2017 *Front. Phys.* **12** 126402
[45] Zuo H B, Zhang M H, Han J C, and Liu J M 2007 *Mater. Lett.* **61** 2697
[46] Cerruti B and Zapperi S 2007 *Phys. Rev. B* **75** 064416
[47] Fan S and Zhong F 2011 *J. Stat. Phys.* **143** 1136
[48] Li Y and Zhong F 2011 arXiv: 1111.1573 [cond-mat.stat-mech]
[49] Zhong F 2012 *Phys. Rev. E* **86** 022104
[50] Lee W, Kim J H, Hwang J G, Noh H R, and Jhe W 2016 *Phys. Rev. E* **94** 032141
[51] Liang N and Zhong F 2017 *Front. Phys.* **12** 126403
[52] Pelissetto A and Vicari E 2017 *Phys. Rev. Lett.* **118** 030602
[53] Liang N and Zhong F 2017 *Phys. Rev. E* **95** 032124
[54] Bar T, Choudhary S K, Ashraf M A, Sujith K S, Puri S, Raj S, and Bansal B 2018 *Phys. Rev. Lett.* **121** 045701
[55] Pal S, Kumar K, and Banerjee A 2020 *Phys. Rev. B* **102** 201109
[56] Qiu L Y, Liang H Y, Yang Y B, Yang H X, Tian T, Xu Y, and Duan L M 2020 *Sci. Adv.* **6** eaba7292
[57] Kundu S, Patel R K, Middey S, and Bansal B 2023 *Phys. Rev. E* **108** 024101
[58] Zhong F 2024 *Chin. Phys. Lett.* **41** 100502
[59] Zhang Y and Zhong F 2025 *J. Phys. Soc. Jpn.* **94** 043001
[60] Zhong F 2025 *Chin. Phys. Lett.* **42** 030203
[61] Zhang Y and Zhong F 2025 *Chin. Phys. Lett.* **42** 090001
[62] Wu Y X, Chen J F, and Quan H T 2025 *Phys. Rev. Lett.* **134** 177101
[63] Chen M, Zhao X H, and Ma Y H 2026 *Phys. Rev. Lett.* **136** 117102
[64] Chen M, Zhao X H, and Ma Y H 2026 *Phys. Rev. E* **113** 034124
[65] Sun Y, Li X, Wang Y, Zhou J, Bai H, and Jin Y 2026 arXiv: 2603.24007 [cond-mat.stat-mech]
[66] Zhang F, Wang Q, Quan H T 2026 arXiv: 2605.06436 [cond-mat.stat-mech]
[67] Sieke L J, Fuchs J, von Smekal 2026 arXiv: 2605.10346 [hep-ph]
[68] Hohenberg P C and Halperin B I 1977 *Rev. Mod. Phys.* **49** 435
[69] Gong S, Zhong F, Huang X, and Fan S 2010 *New J. Phys.* **12** 043036
[70] Zhong F 2011 *Applications of Monte Carlo Method in Science and Engineering* ed Mordechai S (Intech Rijeka) p. 469
[71] Huang Y, Yin S, Feng B, and Zhong F 2014 *Phys. Rev. B* **90** 134108
[72] Feng B, Yin S, and Zhong F 2016 *Phys. Rev. B* **94** 144103
[73] Yuan W, Yin S, and Zhong F 2021 *Chin. Phys. Lett.* **38** 026401
[74] Kramers H A 1940 *Physica* **7** 284
[75] Hanggi, P. Talkner, P. and Borkovec, M. 1990 *Rev. Mod. Phys.* **62** 251
[76] Yang J 2026 Master thesis, Sun Yat-sen University